Phys Chem Minerals (2015) 42:251–260
DOI 10.1007/s00269-014-0716-7

ORIGINAL PAPER

Effects of heat treatment on red gemstone spinel: single-crystal X-ray, Raman, and photoluminescence study

Remo Widmer · Anna-Kathrin Malsy · Thomas Armbruster

Received: 13 July 2014 / Accepted: 10 October 2014 / Published online: 18 October 2014

Abstract A red spinel, $MgAl_2O_4$, from Burma (Myanmar) containing as chromophores ca. 0.5 wt% of each Cr_2O_3 and V_2O_3, was sequentially heated for at least 72 h at temperatures ranging from 600 °C to 1,100 °C. The untreated and quenched samples were examined with single-crystal X-ray diffraction (XRD), Raman spectroscopy and photoluminescence spectroscopy. XRD results display a linear decrease of the cell parameter *a* and a continuous shift of the oxygen coordinate *u, u, u* at 3 *m* toward lower values with increasing temperature and associated Mg, Al disorder: $^{T}(Mg_{1-x}Al_x)^{M}(Al_{2-x}Mg_x)O_4$. The natural spinel has $x = 0.157(2)$ and reaches $x = 0.286(4)$ after quenching from 1,100 °C. In its natural state, M–O and T–O distances are 1.9226(2) and 1.9361(4) Å. With increasing inversion of Mg from the tetrahedrally coordinated T to the octahedrally coordinated M site, M–O distances increase at 1,100 °C to 1.9333(4) Å and T–O distances decrease to 1.9130(8) Å. The crossover temperature, at which T–O and M–O distances become equal (i.e., 1.927 Å), is found to be at 650 °C and corresponds to an inversion parameter $x = 0.208(3)$. With increasing heat treatment, Raman spectra of quenched samples become significantly broadened and a peak characteristic for Mg, Al disorder at 721 cm^{-1} firstly appears for a crystal quenched from 800 °C with $x = 0.248(4)$. At room temperature, photoluminescence spectra are dominated by a strong R line at 684.5 nm accompanied by poorly resolved N lines: N1 (687 nm), N2 (688 nm), and N3 (689 nm). N lines are caused by different Mg, Al environments of Cr^{3+}. With increasing inversion parameter (*x*), the R line decreases in intensity and the N lines become prominent leading to strongly broadened peaks with a maximum shifted toward higher wave lengths (687.5 nm at 1,100 °C). Criteria for the detection of heat treatment on gemstone spinel applicable to gemological routine examination are provided. Extrapolation of *u, a*, and bond lengths from heat-treated Burma spinel toward the natural crystal suggests a retrograde "closing temperature" of ca. 400 ± 100 °C at which Mg, Al disorder was frozen.

Keywords Spinel · $MgAl_2O_4$ · Gemstone · Heat treatment · Mg–Al order–disorder · Single-crystal X-ray · Raman spectroscopy · Photoluminescence spectroscopy

R. Widmer (✉) · T. Armbruster
Mineralogical Crystallography, Institute of Geological Sciences, University of Bern, Freiestrasse 3, 3012 Bern, Switzerland
e-mail: remo.widmer@students.unibe.ch

A.-K. Malsy
Gübelin Gem Lab Ltd., Maihofstrasse 102, 6006 Lucerne, Switzerland

Introduction

Spinel represents a mineral group of the oxide class named after its Al–Mg end-member $MgAl_2O_4$ allowing for a wide range of solid solutions. If being of very good quality in terms of color and transparency, spinel sensu stricto is renowned as precious gemstone. The most popular varieties are of red to pink color. Responsible for the orange and red color are both octahedrally coordinated Cr^{3+} and V^{3+} in trace concentrations (Schmetzer et al. 1989; D'Ippolito 2013). V^{3+}-bearing spinels are characterized by intense absorption bands at ~18,700 cm^{-1} (ν_1) and at ~25,000 cm^{-1} (ν_2), while Cr^{3+}-bearing spinels show two intense and broad bands at similar wavelengths ~18,600 cm^{-1} (ν_1) and ~25,000 cm^{-1} (ν_2). However, the absorption band at ~25,000 cm^{-1} of orange V^{3+}-bearing spinels is wider than the one of Cr^{3+}-bearing spinels. This

causes a stronger absorption in the blue to green regions of the visible spectrum and thus allows for transmittance of orange (D'Ippolito 2013). Hoang et al. (2001) performed annealing experiments on orange–red spinel from Vietnam and reported that the maximum of the $^4A_2 \rightarrow {}^4T_2$ transition shifts from 18,501.4 cm^{-1} (untreated) to 18,148 cm^{-1} (annealed at 920 °C). After heat treatment of an orange–red spinel from Lang Chap (Vietnam) at 850 °C (Malsy et al. 2012), the orange hue decreased and the color changed to the more desired red.

The reasons for color change of gem spinels after heat treatment are multifaceted. If a red spinel also contains very minor Fe as chromophores, the corresponding color may show a magenta-purplish hue (Schmetzer et al. 1989; D'Ippolito 2013). This tint may be altered by the redox conditions of the applied heat treatment influencing the concentrations of tetrahedral and octahedral Fe^{2+}, Fe^{3+}. If Cr^{3+} and V^{3+} are the only chromophores, both characterized by a very high octahedral site preference (Burns 1993; D'Ippolito 2013), the color may be variable depending on the relaxation of the local M–O bond length. Magnesiochromite, $MgCr_2O_4$, and zincochromite, $ZnCr_2O_4$, showing M–O distances of 1.995 Å (Lenaz et al. 2004), and 1.991 Å (Hålenius et al. 2010), respectively, are dark green. If Cr^{3+} is present in trace concentrations in the $Mg(Al_{1-x}Cr_x)_2O_4$ and $Zn(Al_{1-x}Cr_x)_2O_4$ series, with average M–O distances of 1.974 and 1.960 Å, respectively, the color is pale to intensely red (Hålenius et al. 2010). This striking color difference has been related to a different degree of covalency of the local Cr–O bond in Cr dominant and trace-Cr spinels (Hålenius et al. 2010). The same authors also confirmed experiments by (Hoang et al. 2001) that the energy of the spin-allowed ν_1-transition in six coordinated Cr^{3+} ($=10Dq$) in the $Mg(Al_{1-x}Cr_x)_2O_4$ solid solution changes with heat treatment. The local Cr^{3+}-O bond length in a flux grown spinel, $Mg(Al_{1.97}Cr_{0.03})O_4$, was calculated from recorded crystal-field splitting as 1.973(1) Å (Hålenius et al. 2010), while the average M–O bond length was 1.9273 Å (Andreozzi et al. 2000). Both the local (Cr^{3+}) and the average M–O distances lengthen with increasing degree of inversion at high-temperature annealing (Hålenius et al. 2010; Andreozzi et al. 2000).

Red–orange spinels closely resemble ruby in appearance. In Burma, both occur in similar geological environments or even are associated with each other. Their resemblance has led to confusion in the past and many so-called rubies turned out to be spinels only after mineralogists established distinctive chemical and structural features in the last century.

The crucial factor for high-value gemstone spinels is of course their appearance. Not surprisingly, procedures of artificial enhancement were elaborated in order to increase the value of a non-perfect stone. Capable of intensifying, changing or homogenizing color and dissolving small inclusions, heat treatment has already turned out to be effective with regard to ruby and sapphire (Nassau 1984). Consequently, concern had to be raised whether there are undisclosed heat-treated spinels to be found on the market. Studies on characteristics of thermally enhanced stones including photoluminescence and Raman spectroscopy resulted in several distinguishing features (Hoang et al. 2001; Saeseaw et al. 2009). Changes in Raman and photoluminescence spectra after heat treatment have previously been observed (Cynn et al. 1992; Minh and Yang 2004) and are attributed to structural rearrangement during tempering. These findings provide applicable criteria to gemological routine examination. Additional distinguishing features of heated stones, observable by microscopy, are altered mineral inclusion and tension cracks around guest minerals and fluid inclusions. However, gem spinels rarely have observable inclusion, and spectroscopic methods are therefore at an advantage (Malsy et al. 2012).

The study of Malsy et al. (2012) initiated the present investigation with the aim exploring the effects of variable heat treatment on one gemstone spinel by single-crystal X-ray diffraction, photoluminescence spectroscopy, and Raman spectroscopy. X-ray diffraction is applied to monitor variations of average bond length upon heat treatment, which have been shown to influence the energy of "chromophoric" absorption bands (Hålenius et al. 2010), whereas photoluminescence spectroscopy probes the local Cr^{3+} environment.

Specimens of a natural spinel heated progressively at temperatures ranging from 600 to 1,100 °C are analyzed after quenching to room temperature. The results of all three methods are compared and correlated with each other. In addition, based on the temperature dependence of structural parameters, a retrograde "closing temperature" will be estimated for the natural (untreated) Burmese spinel, at which Mg, Al disorder was frozen.

Experimental section

Sample studied

An octahedral red spinel with an edge length of ca. 4 mm, originating from the Mogok gemstone tract in Burma, today's Myanmar (Malsy and Klemm 2010), was cut in (111) slices each 100–150 μm thick. In the Mogok area, red spinels occur in marbles enclosed in biotite–garnet–sillimanite–oligoclase gneisses. Gemstone formation is related to fluid infiltration from an external source with an upper temperature estimate of ca. 700 °C for spinel–forsterite-bearing marble as derived from graphite Raman spectral thermometry (Yui et al. 2008).

Table 1 Experimental setups and structural results

Temp (°C)	Duration (days)	*a* (Å)	*u*	T–O (Å)	M–O (Å)	U_{eq}(O) (Å^2)	*R*1/*wR*2 (%)	*x* inversion
600	30	8.0913 (1)	0.26262 (5)	1.9286 (7)	1.9262 (4)	0.00679 (16)	1.02/2.45	0.199 (4)
650	30	8.0909 (1)	0.26251 (4)	1.9270 (5)	1.9269 (3)	0.00738 (10)	0.94/2.49	0.208 (3)
700	5	8.0908 (1)	0.26224 (5)	1.9232 (7)	1.9288 (3)	0.00735 (13)	0.87/1.90	0.230 (4)
750	3	8.0906 (2)	0.26223 (6)	1.9231 (8)	1.9288 (4)	0.0073 (2)	1.35/2.61	0.230 (4)
800	3	8.0904 (1)	0.26201 (6)	1.9200 (8)	1.9303 (7)	0.0076 (2)	1.29/2.30	0.248 (4)
850	3	8.0902 (1)	0.26193 (5)	1.9188 (7)	1.9309 (4)	0.0079 (2)	1.30/2.53	0.255 (4)
900	3	8.0895 (1)	0.26179 (4)	1.9166 (6)	1.9317 (3)	0.00890 (11)	1.14/2.79	0.266 (3)
1000	3	8.0891 (1)	0.26166 (5)	1.9147 (8)	1.9326 (4)	0.00831 (18)	1.16/2.67	0.276 (4)
1,100	3	8.0888 (1)	0.26154 (5)	1.9130 (8)	1.9333 (4)	0.00829 (14)	1.88/3.36	0.286 (4)
natural	–	8.0919 (1)	0.26314 (3)	1.9361 (5)	1.9226 (2)	0.0052 (1)	1.09/2.41	0.157 (2)

All structure-refinement data with $\sin(\theta)/\lambda > 0.3$. Structural setting: spacegroup *Fd*3 *m*, T at 1/8, 1/8, 1/8, M at ½, ½, ½, O at *u*, *u*, *u*. *Inversion* $x = 21.396–80.714u$ (Andreozzi and Princivalle 2002)

Chemical analyses

Twenty point analyses have been collected on a crystal plate using a JEOL JXA-8230 electron microprobe (EMP) installed at the Yamaguchi University (Japan), operated at 15 kV and 20 nA and applying a beam size of 10 μm. Following standard materials were used: Si and Ca (wollastonite), Ti (rutile), Al (corundum), Cr (eskolaite), V ($Ca_3(VO_4)_2$), Fe (hematite), Mn (MnO), Mg (periclase), Na (albite), K (K-feldspar), Sr and Ba ($SrBaNb_4O_{12}$), Ni (NiO), P ($KTiOPO_4$), F (fluorite), and Cl (halite). In addition, laser ablation inductively coupled plasma mass spectrometry (LA–ICP–MS) measurements were also conducted for quantification of the major color causing transition metal oxides. Experimental conditions are specified by Malsy and Klemm (2010).

Heat treatment

Heating runs with the sample in a platinum crucible were performed in a chamber furnace (VMK 250, Linn High Therm GmbH). The temperature at the target value was kept constant (±1 °C) for variable time under standard pressure in air. Heating and quenching runs were done sequentially in steps of 50 °C from 600 °C up to 900 °C while at intervals of 100 °C from 900 to 1,100 °C. Preliminary test experiments (72 h at 600, 650 and 700 °C) without quenching but after slow cooling in the switched off furnace (cooling rate: ~2 °C/min) yielded unchanged structural parameters and identical spectra to the natural spinel. Thus, in the final experiments, a crystal slice previously heated at 900 °C was sequentially reheated at 600 and 650 °C for 30 days, at 700 °C for 5 days, and at higher temperatures for 3 days. All samples were subsequently quenched in water. An additional sample was heated 3 days at 1,300 °C and water quenched.

Single-crystal X-ray diffraction

After each heating cycle, a crystal of ca. $0.2 \times 0.2 \times 0.15$ mm^3 was harvested from the spinel slice. X-ray diffraction data were collected using an Enraf–Nonius CAD4 diffractometer with κ geometry and point counter. The cell parameters were obtained by least-squares refinements assuming a cubic unit cell (Table 1). These refinements were based on the theta values (Mo$K\alpha_1$) from the same set of 22 reflections for each crystal. This set comprised three strong high-theta ($\theta > 25°$) reflections and some of their symmetry equivalents. The setting angles of each reflection were previously optimized by calculation of the appropriate mean values from a centering procedure at four different positions [+θ, (*hkl*); +θ, (*–h–k–l*); –θ, (*hkl*); –θ, (*–h–k–l*)]. Here, centering a reflection means setting the crystal to the best reflecting position. A half sphere of intensity data in reciprocal space was collected with graphite-monochromated Mo$K\alpha$ X-radiation for each crystal up to $\theta = 35°$. If significant, absorption was corrected by experimental ψ scans collected on selected high χ angle reflections. Structural refinements were performed with the SHELXL program (Sheldrick 2008) using neutral atom scattering factors in space group *Fd* −3 *m* with origin at −3 *m*. The various data sets comprised between 60 and 100 unique reflection with $F_{obs} > 4\sigma$ (F_{obs}) and eight variables. Refinement parameters included scale factor, weighting scheme, secondary extinction coefficient, anisotropic displacement parameters, and oxygen positional parameter *u*. Facing problems with the applied model to properly fit the diffraction data, a second refinement set allowing only reflections with $\sin(\theta)/\lambda > 0.3$ was performed (see "Discussion").

Raman spectroscopy

Raman spectra of the quenched spinel slices were acquired using a Renishaw Raman 1,000 spectrometer coupled with

Table 2 Results of red Burma spinel analyses

Oxide	Average EMP anal.	Esd	Average LA–ICP–MS anal.	Esd
SiO_2	0.16	0.07		
TiO_2	0.12	0.03	0.152	0.003
Al_2O_3	68.98	0.42		
Cr_2O_3	0.67	0.09	0.55	0.07
V_2O_3	0.39	0.05	0.53	0.04
$Fe_2O_3^a$	0.21	0.04	0.016	0.001
MnO	0.01	0.01		
MgO	28.70	0.15		
CaO	0.06	0.04		
SrO	0.01	0.01		
BaO	0.03	0.04		
Na_2O	0.01	0.01		
K_2O	0.01	0.00		
NiO	0.19	0.07		
CuO	0.01	0.01		
ZnO	0.12	0.05	0.034	0.004
P_2O_5	0.01	0.01		
F	0.01	0.02		
Cl	0.00	0.00		
Sum	99.71			

[a] Measured as total Fe

Leica DMLM optical microscope at Gübelin GemLab, Lucern. An argon-ion laser of 514 nm was used allowing for an acquisition time of 60 s for 200–900 cm^{-1} with a resolution of 1.5 cm^{-1}. To provide comparability, intensities of all spectra were normalized to the height of the main peak at about 408 cm^{-1} of the unheated sample. In order to subtract the fluorescence background, a baseline correction was made manually by defining several linear segments.

Photoluminescence spectroscopy

Photoluminescence spectra were obtained between 600 and 800 nm by the same instrument and setup as for the Raman spectra using an acquisition time of 1 s and a spectral resolution of 0.1 nm. Intensities of all spectra were normalized to the height of the peak at about 698 nm of the unheated sample.

Results

Chemical analyses

Average analytical results are presented in Table 2. According to results of average electron microprobe analyses for the major transition metal oxides, the investigated spinel has 0.013(1) Cr, 0.007(2) V, and 0.002(1) Zn pfu (based on 4 O). For Cr and V, results of average LA–ICP–MS analyses agree within 3 esd's. The most obvious difference was found for the Fe_2O_3 content yielding 0.21(4) wt% by EMP analysis but only 0.016(1) wt% by LA–ICP–MS. We interpret the higher Fe_2O_3 content by EMP as an analytical artifact if this difference is not due to local inhomogeneity of the sample.

Single-crystal X-ray diffraction

Structural parameters (Table 1) show considerable dependence if plotted against the heating temperature. The cell parameter a decreases continuously with increasing heat treatment up to 1,100 °C (Fig. 1). Comparing the untreated natural sample with the sample heated at 1,100 °C, a total decrease of a of 0.0031(2) Å is determined. The additional experiment at 1,300 °C yielded the same cell parameter and oxygen coordinate u as for equilibration at 1,100 °C. Kinetic experiments (Andreozzi and Princivalle 2002; Princivalle et al. 2006) suggest that quenching from 1,300 °C with a chamber furnace is not fast enough to preserve the equilibrium state. Thus, the 1,300 °C data were disregarded.

The oxygen parameter u symbolizes the oxygen coordinates u, u, u at the 3 m site of the cubic spinel structure. This parameter shifts with increasing heat treatment up to 1,100 °C (Fig. 2) towards lower values. The overall change of u from the natural spinel to 1,100 °C spans a decrease of 0.00158(6).

In the spinel structure, tetrahedral T–O and octahedral M–O distances are dependent on u and a along with x. For

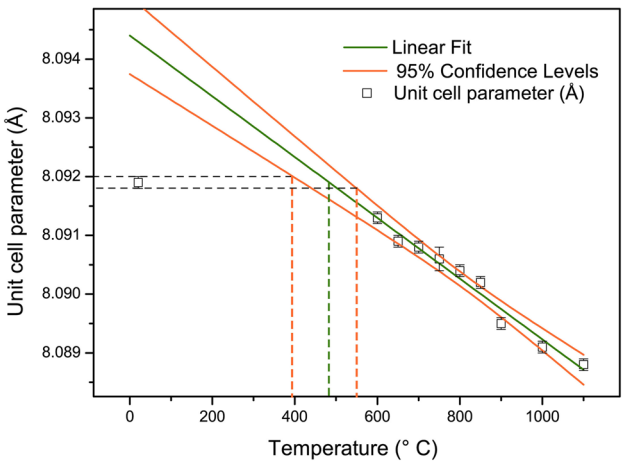

Fig. 1 Temperature dependence of spinel cell dimensions upon heat treatment. The linear regression used for extrapolation to the natural sample is $a = 8.0944–5.1505 \times 10^{-6}$ T (°C), $R^2 = 0.9678$

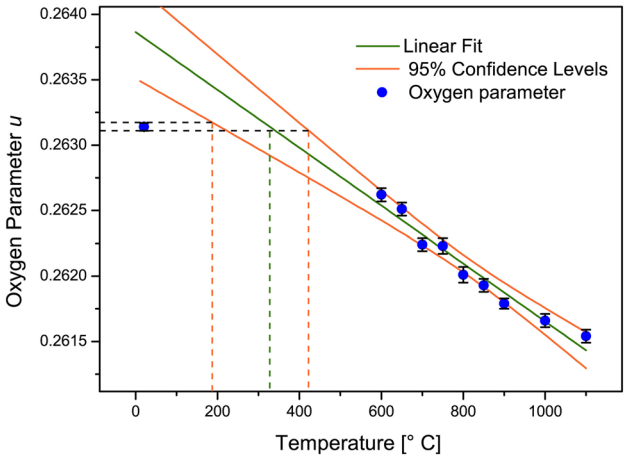

Fig. 2 Temperature dependence of spinel oxygen parameter u upon heat treatment. The linear regression used for extrapolation to the natural sample is $u = 0.2639–2.2279 \times 10^{-6}$ T (°C), $R^2 = 0.9486$

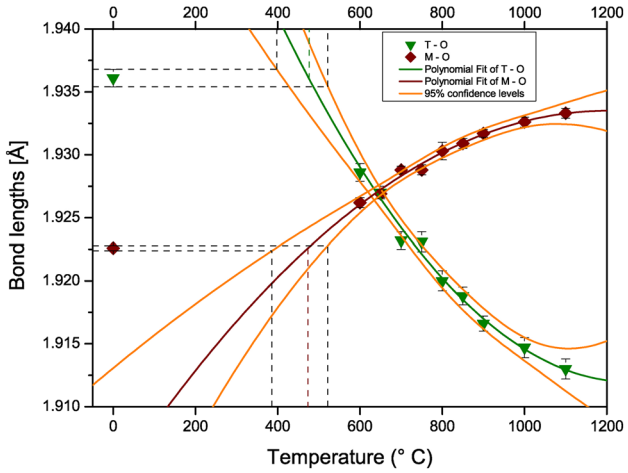

Fig. 3 Temperature dependence of spinel M–O and T–O bond lengths upon heat treatment. The regressions used for extrapolation to the natural sample are T–O = 1.9743–9.30 × 10^{-5} T + 3.95 × 10^{-8} T^2 ($R^2 = 0.985$), M–O = 1.9038–4.937 × 10^{-5} T + 2.05 × 10^{-8} T^2 ($R^2 = 0.979$)

the natural spinel, M–O and T–O distances are 1.9226(2) and 1.9361(4) Å. With increasing inversion of Mg from the tetrahedral T to the octahedral M site, M–O distances increase at 1,100 °C to 1.9333(4) Å and T–O distances decrease to 1.9130(8) Å (Fig. 3). The crossover temperature, at which M–O and T–O distances become equal (1.9270(5) Å), is at 650 °C.

The most sensitive atomic displacement parameter, U_{eq} (O) ($U_{11} = U_{22} = U_{33}$), displays an increase with heating temperature (Fig. 4). Values of atomic displacement parameter of the octahedral position (M) stay more or less constant, whereas values of the tetrahedral position (T) indicate a slight increase with heating.

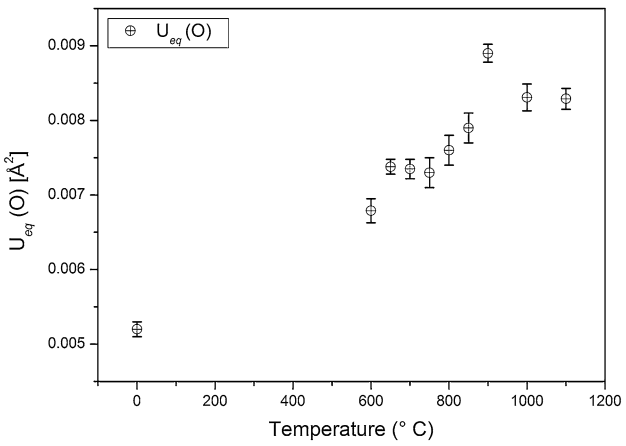

Fig. 4 Temperature dependence of isotropic oxygen displacement parameters of spinel upon heat treatment

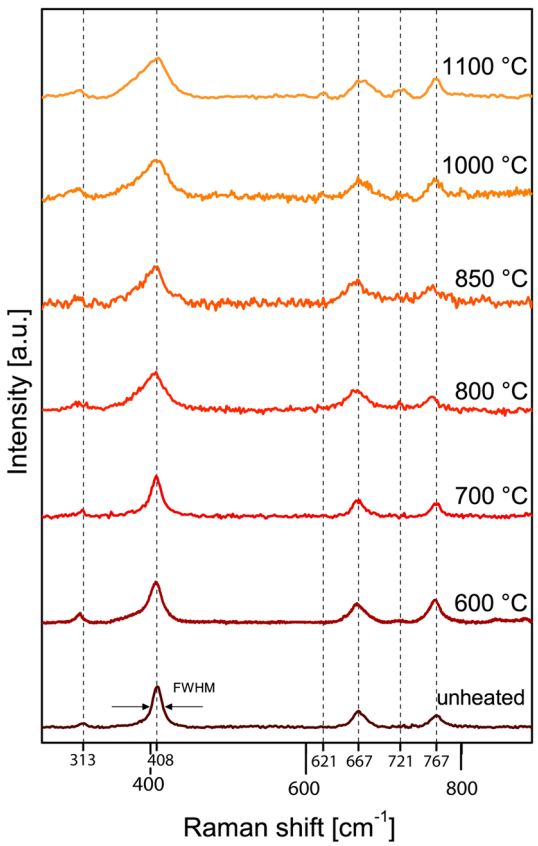

Fig. 5 Raman spectra of natural Burma spinel and after heat treatment. Spectra for 650, 750, and 900 °C were not collected

Raman spectroscopy

Raman spectra are shown in Fig. 5 with major peaks at 408, 665, and 767 cm^{-1}. With increasing heating temperature, all Raman bands widen, which is confirmed by measuring

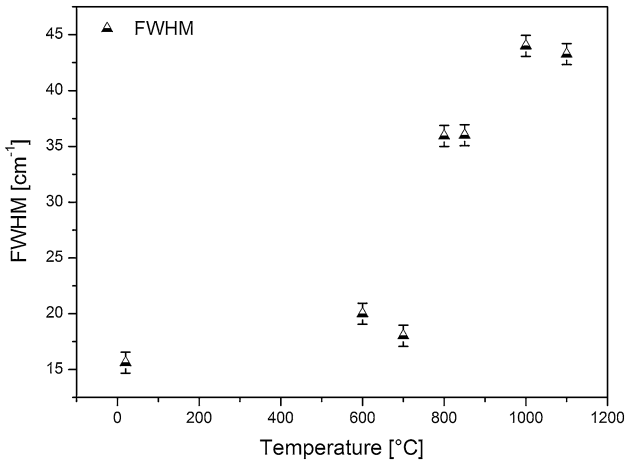

Fig. 6 Broadening (FWHM) of the spinel Raman band at 408 cm^{-1} upon heat treatment. Spectra for 650, 750, and 900 °C were not collected

the full-width at half-maximum (FWHM) values of the main peak near 408 cm^{-1} (Fig. 6). Moreover, a small peak at 314 cm^{-1} continuously shifts toward lower frequencies. An additional peak at 721 cm^{-1} firstly appears for a crystal quenched from 800 °C and prevails up to 1,100 °C. In the spectra of the samples quenched from 1,000 to 1,100 °C, a new weak peak appears at ca. 620 cm^{-1}.

Photoluminescence spectroscopy

The photoluminescence spectra show a remarkable change from rather well-defined peaks of the unheated sample to broadened and poorly defined humps after treatment with increasing temperature (Fig. 7). In order to quantify the evolution of the main peaks, an attempt of gaussian deconvolution in the range from 684 to 690 nm is shown in Fig. 8.

Discussion

There are several powder or single-crystal diffraction studies on $MgAl_2O_4$ spinel after quenching from high temperature or even in situ at high temperature (e.g., Yamanaka and Takéuchi 1983; Peterson et al. 1991; Redfern et al. 1999; Andreozzi et al. 2000; Andreozzi and Princivalle 2002; Méducin and Redfern 2004; Princivalle et al. 2006; Barpanda et al. 2006). Raman spectra at ambient conditions or at high temperature on natural or synthetic $MgAl_2O_4$ spinel (Cynn et al. 1992; Slotznick and Shim 2008; Malsy et al. 2012) and also Cr^{3+} photoluminescence spectra (Wood et al. 1968; Mikenda and Preisinger 1981a, b; Mikenda, 1981; Derkosch and Mikenda 1983; Strek et al. 1988; Phan et al. 2004; Malsy et al. 2012) of natural and synthetic spinel

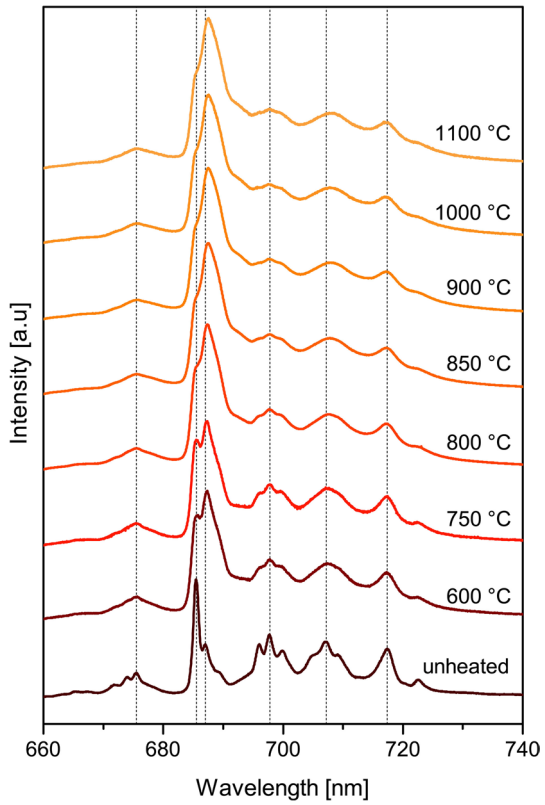

Fig. 7 Cr photoluminescence spectra of Burma spinel unheated and after heat treatment. Spectra for 650 and 700 °C were not collected

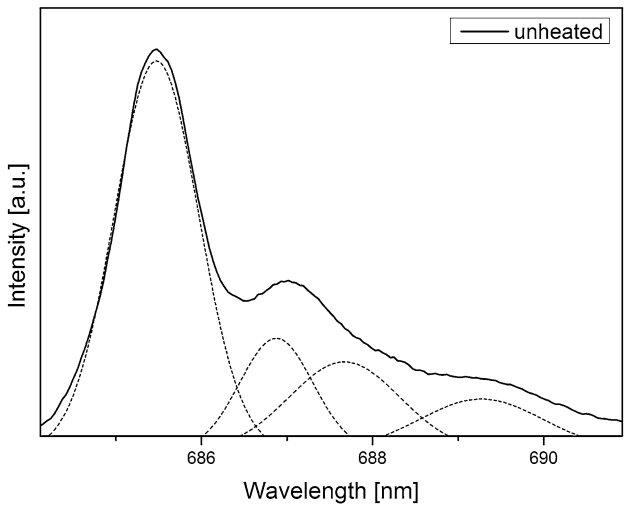

Fig. 8 Cr photoluminescence spectra of untreated Burma spinel: deconvolution of the main band at ca. 684 nm into the R line at 685.4 nm and three overlapping peaks: N1 at 687 nm, N2 at 687.8, and N3 at 689.3 nm

have been repeatedly measured and interpreted. In contrast, the number of combined crystal structure and spectroscopic measurements is scarce (e.g., Malsy et al. 2012). However,

only this methodic combination allows relating long-range order–disorder effects as obtained from the average crystal structure based on diffraction data with short-range effects as monitored by Raman or photoluminescence spectroscopy. By purpose, we applied spectroscopic instruments as commonly used in gemological laboratories, while the single-crystal XRD experiments serve as reference to quantify the order behavior of spinel.

After short-time heating runs between 600 and 700 °C did not show differences to the untreated samples, we used for the long-time treatment in the above temperature range a sample previously "disordered" at 900 °C and re-ordered it by heating it again sequentially to 600, 650, and 700 °C. This procedure is compatible with the kinetic study of Princivalle et al. (2006) on their low-Cr $Mg(Al,Cr)_2O_4$. The latter authors report that their 23 days at 650 °C disordering runs were far from equilibrium and it seems that the time to attain equilibrium would be on the order of thousands of days, too long for most laboratory experiments (Princivalle et al. 2006). In contrast, the ordering experiments at 650 °C performed on the same material but previously disordered 24 h at 1,000 °C took only 4 h to reach equilibrium. Thus, the kinetics for ordering and disordering are strongly different.

Precise single-crystal X-ray studies on gemstone spinel are not straightforward.

(1) The gemmy character of such a hard material (7.5–8 on the Mohs scale) is responsible for a low degree of structural mosaicity giving rise to strong extinction effects. This extinction mainly decreases the intensities of strong low-θ reflections but can be reduced by refining an appropriate extinction parameter.
(2) High-symmetry crystals exhibiting low degree of mosaicity show in diffraction experiments multiple diffraction phenomena ("Umweganregung," Remminger effect). The most obvious implication on the data quality is that low-intensity reflections may exhibit higher intensity than predicted by the model. Multiple diffraction also influences symmetry equivalent reflections to a different extent ($R_{int} > R_\sigma$). Theoretically, this effect can be corrected (e.g., Rossmanith and Armbruster 1995), but there is no routine procedure supplied by standard crystal-structure-refinement packages such as SHELXL (Sheldrick 2008). The influence of multiple diffractions can be reduced by working with small crystals and collecting reflections with high redundancy. The high redundancy takes care that individual reflections, which are severely influenced by multiple diffraction, are not too strongly weighted.
(3) For spinel structure refinements performed on all collected data, the most disagreeable reflection is 222. The observed structure factor (F_o^2) of the 222 reflection appears to be about twice as high as the calculated value F_c^2. A stepwise intensity collection of the rather weak 222 reflection at various psi values confirms that the severe difference between F_o^2 and F_c^2 cannot be assigned to multiple diffraction effects. If the 222 reflection is omitted from the refinement, much better *wR*2 and *GooF* values are achieved. Facing the same problem of poor agreement between observed and calculated F_{222}^2, Della Giusta et al. (1986) applied scattering factors of 50 % ionized elements, Lucchesi and Della Giusta (1997) used scattering curves of fully ionized elements, and Andreozzi et al. (2000) obtained best results in terms of *R*1, *wR*2, and *GooF* using scattering curves of $O^{-1.6}$ and neutral cations.

We applied a strongly simplified structure factor calculation: $F_{hkl}^2 = \left\{ \sum_n f_n \cos 2\pi (hx_n + ky_n + lz_n) \right\}^2$ estimating the influence of variable oxygen scattering factors on the intensity of the 222 reflection. Introducing into the above equation, the atomic positions of an idealized spinel in space group $Fd\,{-}3\,m$ with O at ¼, ¼, ¼ lead to $F_{222}^2 = (16 \times f_M - 32 \times f_{Ox})^2$ where f_M represents the scattering factor of the element in octahedral coordination and f_{Ox} the one of oxygen forming the closest anion packing. Thus, the 222 reflection is independent of the tetrahedral T site. If, e.g., the scattering factor for neutral Al is introduced for f_M (Mo*K*α X-radiation) and f_{Ox} is replaced by either one of the scattering factors for O^0, O^{-1}, and O^{-2}, resulting F_{222}^2 becomes 926, 1,174, and 2,154, respectively. Thus, the dependence of the 222 intensity on the applied structure factor is verified. If the scattering factors of O^0, O^{-1} (Prince 2010), and O^{2-} (Hovestreydt 1983) are plotted *vs.* sin(θ)/λ, it becomes obvious that differences between charged and neutral oxygen scattering factors in routine X-ray data sets are not resolved if $\sin(\theta)/\lambda > 0.3$ corresponding to $d < 1.666$ Å. For this reason, we have excluded this low-θ range in structure refinements presented in this study (six unique reflections were omitted: 111, 022, 113, 222, 004, and 133). This procedure is consistent with electron density studies for which a reference set of "nuclear" coordinates is obtained from a high-θ data set, which is not influenced by valence electrons.

The order–disorder behavior of spinel may be described by the formula $^T(Mg_{1-x}Al_x)^M(Al_{2-x}Mg_x)O_4$ (e.g., Peterson et al. 1991). Spinels with $x = 0$ and $x = 1$ are denoted "normal" and "inverse," respectively. For $x = 0.666$, the Mg and Al distribution is at random. Andreozzi and Princivalle (2002) provide for $MgAl_2O_4$ spinel at equilibrium the simple correlation between x (inversion) and the oxygen parameter u:

$$x = 21.396 - 80.714u.$$

Thus, applying the above equation, the natural Burma spinel (ignoring the influence of minor Cr and V) has $x = 0.157(2)$ and reaches $x = 0.286(4)$ after heat treatment at 1,100 °C. This means that the natural Burma spinel is a "normal" spinel with slight Mg–Al disorder only. This disorder increases with heat treatment, but even after heating at 1,100 °C the spinel remains essentially a "normal" spinel. Notice that the inversion parameter strongly depends on the applied method. ESR (Schmocker and Waldner 1976) and 27Al NMR (Maekawa et al. 1997) usually yield lower inversion parameters (0.05 and below) of gemstone spinels of similar formation conditions as Burmese spinel.

The temperature dependence of our *a* and *u* parameters (Figs. 1, 2) is very similar to the corresponding data of synthetic end-member $MgAl_2O_4$ presented by Andreozzi et al. (2000). Not surprisingly, the intercept of the corresponding regression lines is slightly different because a Cr- or V-bearing spinel has a larger cell dimension than the stoichiometric end-member. However, the slight but systematic difference of the slope for *a* and *u* between our experiments and those of Andreozzi et al. (2000) is striking. The temperature-dependent data for synthetic $MgAl_2O_4$ show a steeper slope compared to Burmese spinel. We do not believe that this difference depends on the chemical composition but rather points to a quenching problem of our high-temperature runs. Inspection of Figs. 1 and 2 indicates that the 900–1,100 °C data define a rather flat slope compared to the remaining data at lower temperature. The vertical furnace used by Andreozzi et al. (2000) allowed water quenching from 1,100 to 400 °C within less than 0.5 s, whereas "several" seconds were needed for sample quenching with a chamber furnace. The quenching hypothesis is also supported by the kinetic ordering data at 900 °C for $MgAl_2O_4$, previously disordered at 1,000 °C (Andreozzi and Princivalle 2002), indicating that ca. 1 min is sufficient to increase Mg, Al order.

With increasing inversion parameter *x*, octahedral M–O bond lengths widen and tetrahedral bond lengths (T–O) shorten (Fig. 3) due to increasing transposition of Mg from T to M and Al from M to T. The statistical mixture of large (Mg) and small (Al) at two sites (M and T), sharing the same oxygen atoms for their coordination polyhedra, leads in the average structure to a significant smearing of the oxygen position depending on the different local Mg, Al environments. In diffraction experiments, this type of oxygen disorder is monitored by the atomic displacement parameter (Kunz and Armbruster 1990). Nevertheless, atomic displacement parameters (Armbruster et al. 1990) are often the "trash cans" of all uncorrected experimental or refinement problems (e.g., absorption, multiple diffraction). Thus, it is not surprising, using different crystal fragments at each temperature step that there are slight "outliers" like our data points at $x = 0.208$ and $x = 0.266$ (Fig. 9).

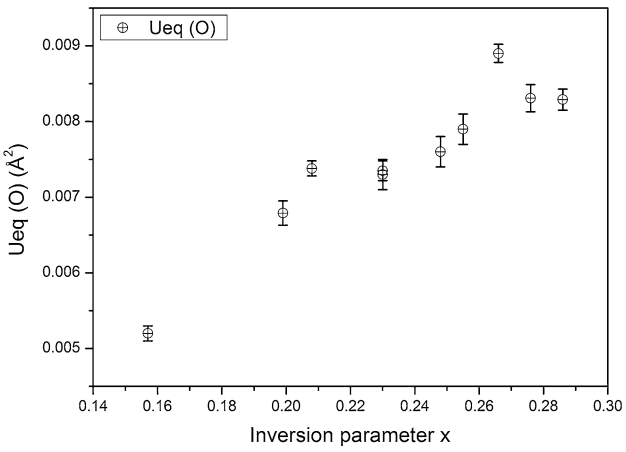

Fig. 9 Dependence of the isotropic oxygen displacement parameters of spinel from the inversion parameter *x*

Andreozzi et al. (2000) observed a similar trend for the temperature dependence of $U_{eq}(O)$ for synthetic $MgAl_2O_4$.

We extrapolated temperature-dependent *u* (oxygen positional parameter) and *a* (cell dimension) data to evaluate an approximate retrograde "closing temperature" for Mg, Al order–disorder of the natural Burmese spinel. However, the agreement between extrapolation of *u* and *a* data is only fair. Extrapolation toward the observed *u* of natural spinel yields ca 320 ± 130 °C (95 % confidence level), whereas cell dimension data suggest ca. 480 ± 90 °C (95 % confidence level). The fair agreement between both approaches is probably due to the linear fit through the data points, although the measurements at 900, 1,000, and 1,100 °C follow a less inclined slope (Figs. 1, 2) as discussed above. Nevertheless, our data points do not deviate more than ca. 2 esd's from the linear regression line. Corresponding though slightly superior linear regressions were also reported by Andreozzi et al. (2000) for heat-treated (600–1,100 °C) synthetic $MgAl_2O_4$ grown by the flux method. Their starting material indicated an order–disorder state characteristic of 800 °C. As an additional approach, we tested a polynomial fit to extrapolate temperature-dependent M–O and T–O distances (Fig. 3), which depend on both *u* and *a*. Results suggest for the natural crystal a retrograde closing temperature of ca. 470 ± 80 °C (95 % confidence level). If we assume that very low Cr + V concentrations in $MgAl_2O_4$ have only negligible effect on the temperature dependence of *u*, the equation ($u = 0.2644–2.7 \times 10^{-6}$ T °C) of Andreozzi et al. (2000) may be applied, and the estimated closing temperature of Burma spinel becomes ca. 480 °C, very close to the value given above. Red spinels from the Mogok area of Myanmar were previously estimated to have formed below 710 °C (Yui et al. 2008).

The Raman spectrum of the natural red Burma spinel consists of four bands: 313 cm^{-1} ($T_{2g}(1)$), 408 cm^{-1} (E_g),

667 cm^{-1} ($T_{2g}(2)$), and 767 cm^{-1} (A_{1g}), which is in excellent agreement with previous studies (e.g., Cynn et al. 1992; Lazzeri and Thibaudeau 2006; Slotznick and Shim 2008). These bands represent octahedral Al and tetrahedral Mg stretching and deformation modes. The broadening on the low wave number tail of the 408 cm^{-1} (E_g) band, which becomes evident after heating to 800 °C and above, was assigned to a bending mode of Al in tetrahedral coordination (Cynn et al. 1992). The additional band at 721 cm^{-1} occurring firstly at 800 °C has been assigned to a fundamental Raman active AlO_4 vibration (Cynn et al. 1992). The weak band at 621 cm^{-1} clearly visible in our spectrum of the spinel quenched from 1,100 °C has hitherto not been described for $MgAl_2O_4$ but appears in other spinels as $F_{2g}(3)$ mode: $MgCr_2O_4$ (Lenaz and Lughi 2013; D'Ippolito 2013), Co_3O_4 (Hadjiev et al. 1988), $ZnGa_2O_4$ (van Gorkom et al. 1973), $ZnCr_2O_4$; $FeAl_2O_4$, $CoAl_2O_4$ (D'Ippolito 2013). In summary, the evolution of Raman spectra with increasing heating temperature probes the Al coordination showing tetrahedral modes only at high temperature. This is consistent with an increase of the inversion parameter *x*.

The Cr^{3+} photoluminescence spectrum for an untreated Burma spinel (Fig. 7) consists of a strong R line (684.5 nm), which actually represents a multiplet of lines (not resolved: separation R1–R2 is ca. 6.5 cm^{-1}, corresponding to 0.3 nm). Sharp zero-phonon R bands originate from the $^2E \rightarrow {}^4A_2$ transition (Wood et al. 1968; Mikenda and Preisinger 1981a) of octahedrally coordinated Cr^{3+} and are accompanied by phonon-sidebands (R-PSB) mirror symmetric to R lines. Luminescence lines, which are neither components of R nor R-PSB lines, are called "N" lines (Wood et al. 1968; Mikenda and Preisinger 1981a, b). In a better resolved spectrum than the routine spectrum measured by us, N1 (687 nm), N2 (688 nm), and N3 (689 nm) decorate the high wavelength tail of the R line (e.g., Wood et al. 1968; Mikenda and Preisinger 1981a). Applying peak deconvolution (Fig. 8) to the spectra of Burma spinel between 684 and 690 nm, in addition to the R line at 685.4 nm, three overlapping peaks could be distinguished: N1 at 687 nm, N2 at 687.8 and N3 at 689.3 nm. Mikenda and Preisinger (1981b) interpret variable R and N line intensities in natural and heated Cr-bearing spinels as caused by different cation environments of octahedral Cr^{3+}.

In a completely ordered $MgAl_2O_4$ spinel with all Mg in tetrahedral (T) and all Al in octahedral (M) coordination (normal spinel), Cr^{3+} has in the first two cation coordination spheres 6 Al^{VI} and 6 Mg^{IV} [a coordination state named Cr(ideal) by Mikenda (1981)]. In this case, the photoluminescence spectrum would only consist of the R and the associated R-PSB lines. With increasing inversion (Al partially occupies T sites and Mg M sites), the probability of Cr(ideal) decreases but other local Cr environments may become more important (e.g., Cr surrounded by 1 Mg and 5 Al at M sites and 4 Mg and 2 Al at T sites). In addition to Cr (ideal), there are 48 possible Cr environments. The observed N lines represent these different Mg, Al disordered Cr surroundings (Mikenda and Preisinger 1981b), and their intensities correspond to the probability of a specific Cr environment.

The dominance of the R line accompanied by N lines indicates that the untreated Burma spinel is a "normal" spinel with "some" Al^{IV}, Mg^{VI} "defects." The relative intensities of the luminescence spectra already changed after long-time heating (30 days) to 600 °C.

The marked broadening of N1 and N3 at 600 °C and above is associated with an increase of N intensity and decrease of R intensity. The N broadening at this heat treatment may be interpreted that there are several slightly different Cr surroundings contributing to these peaks. With increasing temperature, the N lines become more dominant and the R line decreases in intensity.

It is already well known that, e.g., Verneuil-grown (Basso et al. 1991) Cr-doped synthetic spinels can be readily identified by this technique (e.g., Strek et al. 1988). However, it should be kept in mind that such melt-grown spinels are non-stoichiometric and best described as a solid solution between γ-Al_2O_3 and $MgAl_2O_4$ (Basso et al. 1991) with significant octahedral vacancies (ca. 0.2 pfu at M site). For this reason, Verneuil-grown spinels do not exhibit an R line (684.5 nm), but only N lines leading to a broad signal centered at ca. 690 nm (Strek et al. 1988).

Our non-quenched short-time heating experiments 72 h at 600, 650, and 700 °C of Burma spinel indicated that this procedure yielded the same Mg, Al arrangement as the original natural sample, whereas extended heating with subsequent quenching (Table 1) significantly influenced Mg, Al order. Detection of heat treatment by means of diffraction or spectroscopic techniques is only possible if the Mg, Al arrangement is altered by heating. This also suggests that short-time heat treatment below ca. 750 °C of gemstone spinels may not be verified if the degree of inversion remains uninfluenced (e.g., Princivalle et al. 2006; Saeseaw et al. 2009, this study).

Acknowledgments We are highly indebted to Mariko Nagashima (Yamaguchi University, Japan) for performing the electron microprobe analyses. We are grateful to Rosa Micaela Danisi (Bern), Martin Fisch (Bern), and Veronica D'Ippolito (Rome, Italy) for revising a preliminary version of this manuscript. Reviews by Francesco Princivalle (Trieste, Italy) and an anonymous referee are highly appreciated.

References

Andreozzi GB, Princivalle F (2002) Kinetics of cation ordering in synthetic $MgAl_2O_4$ spinel. Am Mineral 87:838–844

Andreozzi GB, Princivalle F, Skogby H, Della Giusta A (2000) Cation ordering and structural variations with temperature in $MgAl_2O_4$ spinel: an X-ray single crystal study. Am Mineral 85:1164–1171

Armbruster T, Bürgi HB, Kunz M, Gnos E, Brönnimann S, Lienert C (1990) Variation of displacement parameters in structure refinements of low albite. Am Mineral 75:135–140

Barpanda P, Behera SK, Gupta PK, Pratihar SK, Bhattacharya S (2006) Chemically induced disorder order transition in magnesium aluminium spinel. J Eur Ceram Soc 26(13):2603–2609

Basso R, Carbonin S, Della Giusta A (1991) Cation and vacancy distribution in a synthetic defect spinel. Z Krist 194:111–119

Burns RG (1993) Mineralogical applications of crystal field theory, 2nd edition. Cambridge University Press, UK 551 p

Cynn H, Sharma SK, Cooney TF, Nicol M (1992) High-temperature Raman investigation of order-disorder behavior in the $MgAl_2O_4$ spinel. Phys Rev B45:500–502

D'Ippolito V (2013) Linking crystal chemistry and physical properties of natural and synthetic spinels: an UV–VIS–NIR and Raman study. PhD Thesis, Sapienza Università di Roma, p 237

Della Giusta A, Princivalle F, Carbonin S (1986) Crystal chemistry of a suite of natural Cr-bearing spinels with $0.15 \leq Cr \leq 1.07$. Neues Jajrb Miner Abh 155:319–330

Derkosch J, Mikenda W (1983) N-lines in the luminescence spectra of Cr^{3+}-doped spinels: (IV) excitation spectra. J Lumines 28:431–441

Hadjiev VG, Iliev MN, Vergilov IV (1988) The Raman spectra of Co_3O_4. J Phys C: Solid State Phys 21:L199–L201

Hålenius U, Andreozzi GB, Skogby H (2010) Structural relaxation around Cr^{3+} and the red-green color change in the spinel (sensu stricto)-magnesiochromite ($MgAl_2O_4$–$MgCr_2O_4$) and gahnite-zincochromite ($ZnAl_2O_4$–$ZnCr_2O_4$) solid-solution series. Am Mineral 95:456–462

Hoang LC, Khoi NT, Quang VX, Minh NV, Jaing CC (2001) Some optical properties of Vietnam natural spinel. Proc. internat. workshop on material characterization by solid state spectroscopy: gems and minerals of Vietnam, Hanoi, 200–209

Hovestreydt E (1983) On the atomic scattering factor for O^{2-}. Acta Crystallogr A39:268–269

Kunz M, Armbruster T (1990) Difference displacement parameters in alkali feldspars: effects of (Si, Al) order-disorder. Am Mineral 75:141–149

Lazzeri M, Thibaudeau P (2006) *Ab initio* Raman spectrum of the normal and disordered $MgAl_2O_4$ spinel. Phys Rev B74: 140301,1-140301,4

Lenaz D, Lughi V (2013) Raman study of $MgCr_2O_4$–$Fe^{2+}Cr_2O_4$ and $MgCr_2O_4$–$MgFe_2{}^{3+}O_4$ synthetic series: the effects of Fe^{2+} and Fe^{3+} on Raman shifts. Phys Chem Minerals 40:491–498

Lenaz D, Skogby H, Princivalle F, Hålenius U (2004) Structural changes and valence states in the $MgCr_2O4$–$FeCr_2O_4$ solid solution series. Phys Chem Minerals 31:633–642

Lucchesi S, Della Giusta A (1997) Crystal chemistry of a highly disordered Mg–Al natural spinel. Mineral Petrol 59:91–99

Maekawa H, Kato S, Kawamura K, Yokokawa T (1997) Cation mixing in natural $MgAl_2O_4$ spinel: a high temperature 27Al NMR study. Am Mineral 82:1125–1132

Malsy A-K, Klemm L (2010) Distinction of gem spinels from the Himalayan Montain Belt. Chimia 64:741–746

Malsy A-K, Karampelas S, Schwarz D, Klemm L, Armbruster T, Tuan DA (2012) Orange–red to orange–pink gem spinels from a new deposit at Lang Chap (Tan Huong-Truc Lau). Vietnam. J Gemmol 33:19–27

Méducin F, Redfern SAT (2004) Study of cation order-disorder in spinel by in situ neutron diffraction up to 1600 K and 3.2 GPa. Am Mineral 89:981–986

Mikenda W (1981) N-lines in the luminescence spectra of Cr^{3+}-doped spinels: (III) partial spectra. J Lumines 26:85–98

Mikenda W, Preisinger A (1981a) N-lines in the luminescence spectra of Cr^{3+}-doped spinels: (I) identification of N-lines. J Lumines 26:53–66

Mikenda W, Preisinger A (1981b) N-lines in the luminescence spectra of Cr^{3+}-doped spinels: (II) origins of N-lines. J Lumines 26:67–83

Minh NV, Yang I-S (2004) A Raman study of cation-disorder transition temperature of natural $MgAl_2O_4$ spinel. Vibr Spec 35:93–96

Nassau K (1984) Gemstone Enhancement. Butterworths, p 272

Peterson RC, Lager GA, Hitterman RL (1991) A time-of-flight powder diffraction study of $MgAl_2O_4$ at temperatures up to 1273 k. Am Mineral 76:1455–1458

Phan T-L, Yu S-C, Phan M-H, Han TPJ (2004) Photoluminescence properties Cr^{3+}-doped $MgAl_2O_4$ natural spinel. J Korean Phys Soc 45:63–66

Prince E. (2010) International Tables for Crystallography, Vol C, Wiley, p 1000

Princivalle F, Martignago F, Dal Negro A (2006) Kinetics of cation ordering in natural Mg(Al, Cr3+)2O4 spinels. Am Mineral 91:313–318

Redfern SAT, Harrison RJ, O'Neill H, St C, Wood DRR (1999) Thermodynamics and kinetics of cation ordering in MgAl2O4 spinel up to 1600°C from in situ neutron diffraction. Am Mineral 84:299–310

Rossmanith E, Armbruster T (1995) The intensity of forbidden reflections of pyrope: umweganregung or symmetry reduction? Z Kristallogr 210:645–649

Saeseaw S, Wang W, Scarratt K, Emmett JL, Douthit TR (2009) Distinguishing heated spinels from unheated natural spinels and from synthetic spinels: a short review of on-going research. http://www.giathai.net/pdf/Heated_spinel_Identification_at_May_25_2009.pdf. Retrieved 07/01/2014

Schmetzer K, Haxel C, Amthauer G (1989) Colour of natural spinels, gahnospinels and gahnites. N Jajrb Miner Abh 160:159–180

Schmocker U, Waldner F (1976) The inversion parameter with respect to the space group of $MgAl_2O_4$ spinels. J Phys C9:235–237

Sheldrick GM (2008) A short history of SHELX. Acta Cryst A64:112–122

Slotznick SP, Shim S-H (2008) In situ Raman spectroscopy measurements of MgAl2O4 spinel up to 1400°C. Am Mineral 93:470–476

Strek W, Derén P, Jezowska-Trzebiatowska B (1988) Optical properties of Cr^{3+} in $MgAl_2O_4$ spinel. Physica B152:379–384

Van Gorkom GGP, Haanstra JH, v d Boom JH (1973) Infrared and Raman spectra of the spinel $ZnGa_2O_4$. J Raman Spec 1:513–519

Wood DL, Imbusch GF, Macfarlane RM, Kisliuk P, Larkin DM (1968) Optical spectrum of Cr^{3+} ions in spinels. J Chem Phys 48:5255–5263

Yamanaka T, Takéuchi Y (1983) Order-disorder transition in $MgAl_2O_4$ spinel at high temperatures up to 1700°C. Z Kristallogr 165:65–78

Yui T-F, Zaw K, Wu C-M (2008) A preliminary stable isotope study on Mogok ruby Myanmar. Ore Geol Rev 24:192–199